Applied Materials Today 21 (2020) 100820

Contents lists available at ScienceDirect

Applied Materials Today

journal homepage: www.elsevier.com/locate/apmt

In situ electrochemical conversion of cobalt oxide@MOF-74 core-shell structure as an efficient and robust electrocatalyst for water oxidation

Wei Gao[a], Wangyan Gou[a], Renjie Wei[b], Xiuming Bu[b], Yuanyuan Ma[a,*], Johnny C. Ho[b,c,d,**]

[a] State Key Laboratory of Solidification Processing, Center for Nano Energy Materials, School of Materials Science and Engineering, and School of Chemistry and Chemical Engineering, Northwestern Polytechnical University and Shaanxi Joint Laboratory of Graphene (NPU), Xi'an 710072, China
[b] Department of Materials Science and Engineering, City University of Hong Kong, 83 Tat Chee Avenue, Kowloon, Hong Kong
[c] State Key Laboratory of Terahertz and Millimeter Waves, City University of Hong Kong, 83 Tat Chee Avenue, Kowloon, Hong Kong
[d] Key Laboratory of Advanced Materials Processing & Mold (Zhengzhou University), Ministry of Education, Zhengzhou 450002, China

ARTICLE INFO

Article history:
Received 29 July 2020
Revised 27 August 2020
Accepted 4 September 2020

Keywords:
Electrocatalysis
Metal-organic framework
In situ activation
Oxygen evolution
Cobalt oxide

ABSTRACT

In recent years, applications of metal-organic frameworks (MOFs) in electrocatalysis, including hydrogen and oxygen evolution reactions, have attracted increasing attention for renewable energy conversion. Herein, the fabrication of core-shell structured Co_3O_4@MOF-74 catalysts is proposed and realized with the tunable thickness of MOF shell layers, where Co_3O_4 nanowire arrays prefabricated on Ni foam are employed as the template as well as the metal source to react with organic ligands to achieve the MOF layers. Importantly, the optimized Co_3O_4@MOF-74 structures exhibit much enhanced catalytic activities towards oxygen evolution reaction (OER), requiring an impressively low overpotential of 285 mV to afford a current density of 50 mA cm^{-2} together with a small Tafel slope of 43 mV/dec, as compared with the pristine Co_3O_4 sample. By investigating the Co_3O_4@MOF-74 structure after OER stability test, the conversion of MOF-74 into cobalt hydroxide shell layers is thoroughly characterized and confirmed, suggesting the *in situ* electrochemical conversion of MOF structures during the electrochemical process. All these results do not only uncover the changes in crystalline and chemical structures of MOFs for electrocatalytic reactions, but also help to comprehend and design novel MOFs as efficient and robust electrocatalysts for practical utilization.

1. Introduction

Electrocatalytic oxygen evolution reaction (OER), also known as water oxidation, is an important half-reaction for applications in water electrolysis and rechargeable metal-air battery; however, it is a sluggish and complex process for the conversion between electrical and chemical energies, requiring highly active and robust noble-metal anode catalysts. [1–3] Since then, low-cost transition metal-based electrocatalysts (*e.g.* Co-based materials as the electrodes for water electrolysis) have been extensively explored as effective alternatives to these noble-metal catalysts. [4, 5] Very recently, another new class of materials, metal-organic frameworks (MOFs), have been widely considered as novel catalyst candidates for various heterogeneous catalytic reactions because of their advantages of high porosity, large surface areas, abundant active metal sites and tunable functionalized linkers. [6–9] Preparation of nanosized catalysts with the compositions of alloys, oxides, sulfides, phosphides, selenides and such from MOFs by post-treatment has been broadly investigated. [10,11,13–17,19] In order to prepare these MOF-derived electrocatalysts, high temperature treatments are generally adopted to form metal-based compounds, accompanied with the carbonization of linkers and ligands and collapse of the original MOF structures.

In addition to MOFs-derived structures, direct applications of transition metal-based MOFs and their integration with other materials as advanced electrocatalysts have been also proposed and realized; this way, the advantages of high porosity and plentiful active metal sites of MOF structures can be fully utilized. [20–24] Various single and multi-component metal-based (*e.g.* Fe, Co, Ni, Mn and Cu) MOFs are hence developed as electrocatalysts for different electrochemical reactions, such as hydrogen evolution, oxygen evolution, oxygen reduction and so on. [25,33,35,37–39,41,43,45,46] For example, Zhao et al. reported the excellent activity of ultrathin nanosheets of NiFe-based MOF arrays supported on Ni foam as bifunctional electrocatalysts for both hydrogen and oxygen evolution reactions in alkaline solution.

* Corresponding author.
** Corresponding Author.
E-mail addresses: yyma@nwpu.edu.cn (Y. Ma), johnnyho@cityu.edu.hk (J.C. Ho).

https://doi.org/10.1016/j.apmt.2020.100820
2352-9407/

[28] Moreover, the wide diversity of ligands and linkers makes it efficient to design and modulate the structural, electronic and physiochemical properties of MOFs. Several typical ligands, including 1,4-benzenedicarboxylate (or 1,4-benzenedicarboxylic acid, BDC), 2,5-dihydroxyterephthalate (or 2,5-dihydroxyterephthalic acid, H_4DOBDC), 1,3,5-benzenetricarboxylic acid (or BTC), and 2-methylimidazole (or MeIM) have been employed to construct transition metal-based MOFs, such as ZIF-67, and MOF-74 that can function as efficient electrocatalysts. [12, 19, 32, 36, 40, 44] The coordination between divalent transition metals and H_4DOBDC constructed the family of MOF-74 with a general formula of $M_2(H_4DOBDC)(H_2O)_2$ (*M*= Mg, Mn, Fe, Co, Ni, and Zn). [18] Structural features of one-dimensional channels with aperture diameters of around 1 nm, different divalent metals nodes and corresponding bonding strengths with H_4DOBDC ligands enabled their applications in electrocatalysis. Unfortunately, there are still substantial challenges in achieving sufficient conductivity and chemical stability for the practical deployment of MOF structures for electrocatalysis. [30, 47] In this regard, rational design of MOF structures and their composites are required to overcome the above issues and to further boost up their electrocatalytic properties.

At the same time, employing the transition metal-based nanostructures as the templates to epitaxially fabricate MOF layers has been lately established as a facile method to not only improve their conductivity but also make the best use of their intrinsic properties for practical utilization. [19,48,53–55] Typically, the ZnO@ZIF-8 core-shell structured sensor was *in situ* fabricated from the surface reaction between dissolved Zn^{2+} ions from ZnO and ligand in solvents to form the outlayer of MOF. [53] Herein, we successfully prepare the Co_3O_4@MOF-74 core-shell structure by using the Co_3O_4 nanowire arrays on Ni foams as the templates as well as also the material cores, while the cobalt-based MOF-74 serves as the outer shell layers. Simply by controlling the solvothermal cycles, the thickness of MOF-74 shell layers can be easily regulated between 4.5 and 17.8 nm. When configured as the anode catalysts for OER, the Co_3O_4@MOF-74 on Ni foam electrocatalysts exhibit the significantly improved activity. The best-performed Co_3O_4@MOF-74 sample yields an impressively low overpotential of only 285 mV to drive a current density of 50 mA cm^{-2} with a Tafel slope of 43 mV/dec, as compared with the pure Co_3O_4 on Ni foam (337 mV and 76 mV/dec, respectively). Further characterization suggests the MOF-74 shells would be self-converted into cobalt hydroxide layers during OER process, which can be attributed to the *in situ* electrochemical activation of MOF layers to become cobalt hydroxides as the active catalytic centers in alkaline solution. All these results evidently indicate that the highly active and stable electrocatalysts can be achieved by the *in situ* electrochemical conversion of Co_3O_4@MOF-74 into Co_3O_4@$Co(OH)_2$ core-shell structures for efficient water oxidation.

2. Experimental section

2.1. Materials preparation

Preparation of Co_3O_4 nanowire arrays on Ni foams. Co_3O_4 nanowire arrays on Ni foams were prepared by using the simple hydrothermal method followed by thermal annealing. Typically, Ni foam pieces (purchased from Suzhou Taili Material Technology Company, China, 1 × 3 cm) were washed with 10% diluted HCl solution, water and ethanol successively with ultrasonication, and then dried at 60 °C. Then, the Ni foams were placed into a 20 mL Teflon-lined autoclave with a 15 mL mixture solution containing 1 mmol of $Co(NO_3)_2$•$6H_2O$, 1 mmol of NH_4F and 1 mmol of urea. The autoclave was sealed and next heated at 120 °C for 8 h in an electrical oven. After cooling to room temperature, the as-prepared precursor was washed with distilled water and ethanol alternatively for several times, and then dried at 60 °C. The Co_3O_4 nanowire arrays on Ni foams were eventually obtained by annealing the above precursor at 300 °C with a temperature ramping rate of 5 °C/min for 2 h in air.

Preparation of the Co_3O_4@MOF-74 core-shell structure. To coat the MOF-74 layer on Co_3O_4, the solvothermal method was adopted without adding any metal salts. Typically, a piece of Co_3O_4/Ni foam (1 × 1.5 cm) was placed into a 20 mL Teflon-lined autoclave containing 5 mg of 2,5-dihydroxyterephthalic acid (H_4DOBDC) and 10 mL of *N,N*-dimethylformamide (DMF). Then, the autoclave was sealed and heated at 150 °C for 10 h. After reaction, the sample was washed with ethanol and DMF alternatively, and then dried in the vacuum oven. To increase the thickness of MOF-74 layer, the above-mentioned solvothermal process was repeated for several cycles with the same amount of H_4DOBDC in DMF.

2.2. Characterizations

Transmission electron microscopy (TEM) images were obtained from a Hitachi 7700 microscope with an accelerating voltage of 120 kV and high-resolution TEM (HRTEM) images were collected using a JEOL JEM 2100F microscope with an accelerating voltage of 200 kV. Scanning electron microscopy (SEM) images were acquired from a Philips LX 30 FEG microscope with an accelerating voltage of 20 kV. X-ray diffraction (XRD) patterns were measured using a Rigaku powder X-ray diffractometer with the Cu Kα radiation. X-ray photoelectron spectra (XPS) were collected from an X-ray photoelectron spectroscopy system (ULVAC-PHI Inc., model 5802, Kanagawa, Japan) with Cu Kα as the excitation source. Fourier transform infrared (FTIR) analyses were acquired using a Thermo Scientific Nicolet 6700 Fourier transform infrared spectroscopy.

2.3. Electrochemical measurements

All the electrochemical tests were performed on a CHI 660D electrochemical workstation using a three-electrode setup to measure the activity and stability of various samples, where the as-prepared samples on Ni foam, Ag/AgCl (3 M KCl) electrode and graphite rod were employed as the working electrode, reference electrode and counter electrode, correspondingly. The active geometric areas of various samples immersing into the electrolyte were defined by sealing with the silicone rubber. Before linear sweeping voltammetry (LSV) measurement, 10 cyclic voltammetry (CV) cycles were performed first. Then, the LSV method was used with a scan rate of 10 mV/s in 1.0 M KOH solution to obtain the polarization curves at room temperature. The stability tests of electrocatalysts for OER were performed using chronoamperometry method with a fixed overpotential of 400 mV. The potential scale with respect to reverse hydrogen electrode (RHE) was corrected by the Nernst equation, where $E_{vs\ RHE} = E_{vs\ Ag/AgCl\ (3\ M\ KCl)} + 0.0592 \times pH + 0.197$ (V). Electrochemical impedance spectroscopy (EIS) was measured under a fixed overpotential of 400 mV with a frequency range between 100 kHz to 0.1 Hz. All polarization curves were iR corrected unless otherwise mentioned. The produced amount of oxygen gas was measured under a fixed current density of 50 mA cm^{-2}, using a gas chromatography (Techcomp GC 7900) with the thermal conductivity detector, whereas the Faradaic efficiency was calculated from the measured amount of oxygen and the theoretical value of oxygen.

3. Results and discussion

The preparation process of Co_3O_4@MOF-74 core-shell structures is depicted in **Scheme 1**. To be specific, Co_3O_4 nanowire arrays are

Scheme 1. Synthesis schematic for the *in situ* transformation of Co_3O_4 into Co_3O_4@MOF-74.

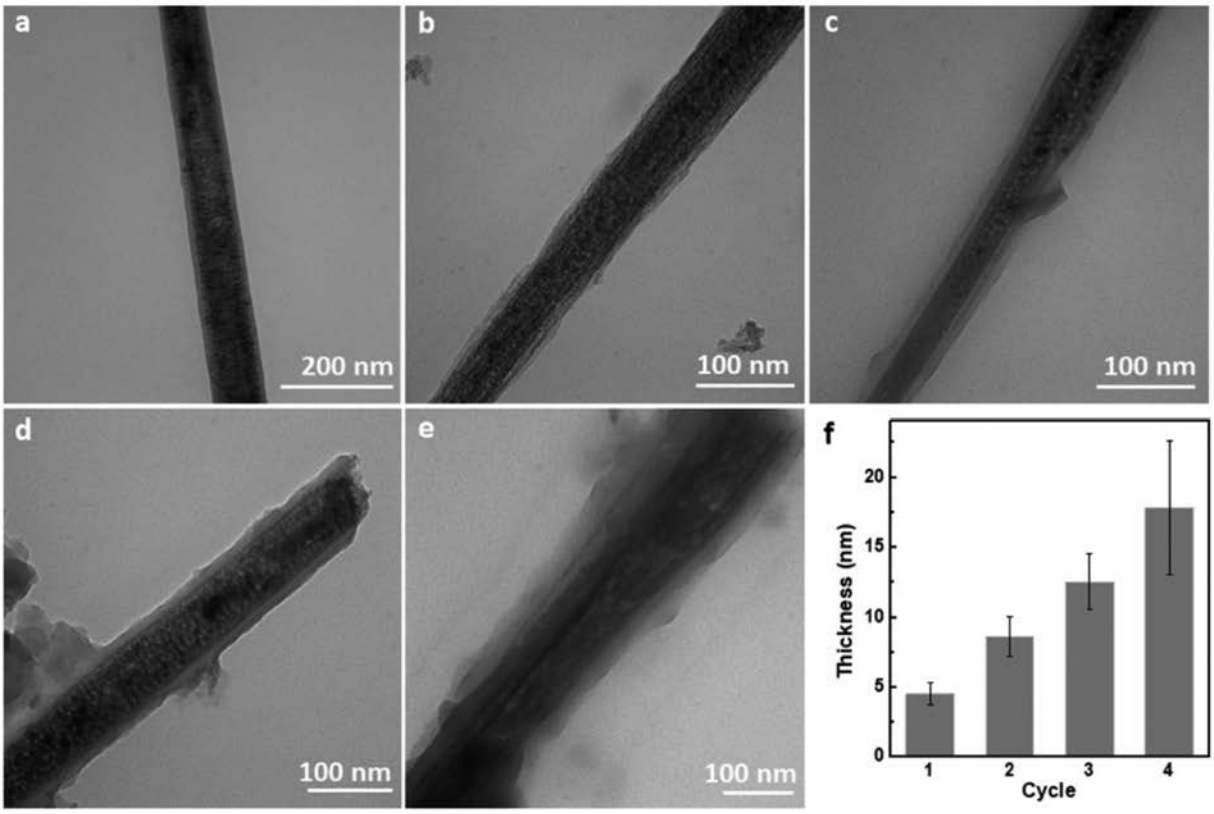

Fig.. 1. Typical TEM images of (a) Co_3O_4 nanowire, Co_3O_4@MOF-74 with (b) 1 solvothermal cycle, (c) 2 solvothermal cycles, (d) 3 solvothermal cycles and (e) 4 solvothermal cycles. (f) The dependence of the MOF layer thickness with various solvothermal cycles.

first fabricated on Ni foams as the templates as well as the material cores by the hydrothermal method followed by the thermal annealing in ambient air. **Figure S1** shows the typical SEM images of well-aligned Co_3O_4 nanowire arrays successfully grown on Ni foams, while **Fig. 1a** presents the TEM image demonstrating the uniform nanowire morphology of Co_3O_4 with the length of several micrometers and the width of about 100 nm. As revealed in the XRD pattern in **Fig. 2**, the nanowire arrays are confirmed to have the cubic Co_3O_4 structure (PDF #43–1003). After that, the cobalt-based MOF-74 shell layers are fabricated on the Co_3O_4 nanowire templates by the solvothermal method using H_4DOBDC as the ligand and Co_3O_4 as the metal source without adding any other metal salts. The etching of Co_3O_4 nanowires by H_4DOBDC would result in Co ions on the surface of Co_3O_4, followed by the surface chemical reaction between H_4DOBDC and surface Co ions for the formation of MOF-74 layers [53]. After one solvothermal cycle, there is an apparent shell layer with a thickness of 4.5 ± 0.8 nm ob-

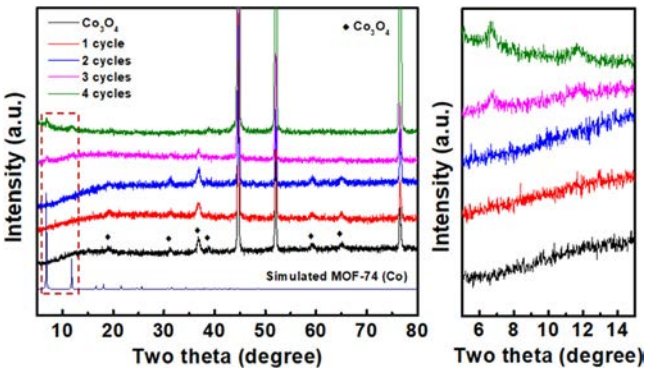

Fig.. 2. XRD patterns of Co_3O_4 and Co_3O_4@MOF-74 with various solvothermal cycles.

served in the TEM image (**Fig. 1b**). However, due to the low material content of MOF-74, there are not any clear peaks indexed to the MOF-74 structure in the XRD spectrum (**Fig. 2**). In order to have a better knowledge on the formation of MOF-74 layers, different solvothermal cycles are performed to regulate the thickness of MOF-74 shell layers using the identical reaction condition. It is obvious that the thickness of Co_3O_4@MOF-74 layers gets increased from 4.5 ± 0.8 nm to 8.6 ± 1.4, 12.5 ± 2.0 and 17.8 ± 4.8 nm when the reaction cycle is implemented for 1 to 4 times, respectively (**Fig. 1b-1f**). SEM images also confirmed the increased coating of MOF-74 layers on the Co_3O_4 nanowire arrays after various cycles (**Figure S2**). Notably, there are not any noticeable particles aggregated onto the nanowires for the samples after 1 and 2 reaction cycles (**Figure S2a** and **S2b**). In contrast, large nanoparticles of MOF-74 are witnessed on the nanowire surface for the samples after 3 and 4 reaction cycles (**Fig. 1c** and **1d, Figure S2c**), which suggests the detachment of Co ions from Co_3O_4 nanowires, followed by the epitaxial growth and migration of MOF-74 to the outer radial region of nanowires. Furthermore, there is an enhancing intensity for the XRD peaks located at about 6.7° and 11.7° for the increasing MOF-74 shell thickness, where the peak locations are consistent with the simulated Co-based MOF-74 structure (**Fig. 2**). [56] Meanwhile, the signals that indexed to Co_3O_4 decrease gradually as the result of the growth of MOF-74 layers. All these results indicate that the MOF-74 shell layers are evidently deposited onto the Co_3O_4 nanowire surface by *in situ* conversion reaction, where H_4DOBDC functioned as the ligand and Co_3O_4 nanowires worked as the metal source as well as the hard templates to support the obtained MOF-74 shells.

The surface chemical states of Co and O in Co_3O_4@MOF-74 are analyzed by XPS to assess their changes before and after introducing the MOF layers. For pristine Co_3O_4, there are obvious peaks of Co $2p_{3/2}$ and $2p_{1/2}$ observed at 779.8 and 795.2 eV, respectively, which are ascribed to the oxidized Co species (**Figure S3a**). The additional peaks witnessed at 785.1 and 802.0 eV are related to the satellite peaks of Co, matching well with those in previous reports. [57] Co_3O_4@MOF-74 with various solvothermal cycles exhibited positive shifts in the binding energy for Co $2p_{3/2}$ signals as compared to pristine Co_3O_4, depicting the interaction between the Co_3O_4 core and the MOF-74 shell. Particularly, the most significant up-shift in the Co $2p_{3/2}$ peak of about 0.6 eV is revealed for Co_3O_4@MOF-74 grown with 2 solvothermal cycles as compared with Co_3O_4, indicating the strong interaction between Co_3O_4 and MOF-74. Similarly, for O 1 s spectra, there are negative shifts in the binding energy for all Co_3O_4@MOF-74 samples as compared with pristine Co_3O_4, where the Co_3O_4@MOF-74 sample grown with 2 solvothermal cycles has the maximum down-shift of about 0.3 eV, suggesting the electron-rich states of oxygen for Co_3O_4@MOF-74 (**Figure S3b**). Therefore, the strong interaction between the Co_3O_4 core and the MOF-74 shell can significantly affect and regulate the electronic structure of Co species, which is anticipated to have the substantial influence on their catalytic performance for OER.

In addition, FTIR spectra of pristine Co_3O_4 and Co_3O_4@MOF-74 grown with 2 solvothermal cycles are measured to further demonstrate the MOF-74 shell coated on the Co_3O_4 nanowire core (**Figure S4**). For pristine Co_3O_4, a strong peak observed at 651 cm^{-1} is corresponded to the Co^{2+}—O vibration with the tetrahedral structure in Co_3O_4 [58, 59]. Another peak located at 1636 cm^{-1} is ascribed to the existence of absorbed molecular water. [59] In fact, for the Co_3O_4@MOF-74 sample grown with 2 solvothermal cycles, the Co^{2+}—O vibration peak at 651 cm^{-1} is also observed because Co_3O_4 functions as the material core in this core-shell structure, while several new peaks are detected owing to the formation of MOF-74 shell layers. Specifically, the peaks located at 815 and 885 cm^{-1} are associated with the C–H wagging, in-plane and out-of-plane of bending modes of the benzene ring, whereas those centered at 1117 and 1198 cm^{-1} are assigned to the in-plane deformation of C–H bond in the benzene ring. The feature at 1413 cm^{-1} is caused by the stretching vibration of $C = C$ bond in the benzene ring. The peak at 1560 cm^{-1} is related to the asymmetric vibration of carboxylate group in the ligand. The signal at 1242 cm^{-1} is corresponded to the C–N vibration of absorbed DMF solvent on the surface of MOF structure or in its channels. [56, 59] All these feature peaks observed for Co_3O_4@MOF-74 further confirm the formation of MOF-74 shell layers, being perfectly consistent with the XRD results discussed before.

To shed light on the effect of coating these MOF shell layers on the catalytic properties towards OER, detailed electrochemical characterizations are performed in 1.0 M KOH solution using pristine Co_3O_4 and Co_3O_4@MOF-74 with different solvothermal cycles as the working electrodes. For Co_3O_4@MOF-74 electrocatalysts, they are first activated by carrying out 10 CV cycles, where the typical details for Co_3O_4@MOF-74 grown with 2 solvothermal cycles are given in **Figure S5**. Polarization curves with iR correction after the activation of 10 CV cycles are exhibited in **Fig. 3a**. The corresponding Tafel slopes derived from the polarization curves are shown in **Fig. 3b**. It is clear that the pristine Co_3O_4 requires an overpotential of 336 mV to reach a current density of 50 mA cm^{-2} with a relatively large Tafel slope of 76 mV/dec determined. On the contrary, all the Co_3O_4@MOF-74 electrocatalysts exhibit the better performance than the pristine Co_3O_4 with lower overpotentials and smaller Tafel slopes (**Fig. 3c**). When the solvothermal process is implemented for 1 to 4 cycles, the Co_3O_4@MOF-74 catalysts only need overpotentials of 299, 285, 310 and 318 mV to achieve a current density of 50 mA cm^{-2} together with Tafel slopes of 65, 43, 53 and 66 mV/dec, respectively. Among all the investigated electrocatalysts, the Co_3O_4@MOF-74 samples grown with 2 solvothermal cycles have the best performance with the smallest overpotential and Tafel slope because of its optimal thickness of MOF shell. These particular samples are then selected as the representative Co_3O_4@MOF-74 catalysts for subsequent studies with the aim to understand the performance enhancement of introducing the MOF-74 shell layers.

As illustrated in **Fig. 4a**, the Co_3O_4@MOF-74 catalysts require an overpotential of 285 mV, while the pristine Co_3O_4 need a larger overpotential of 336 mV to obtain the same current density of 50 mA cm^{-2}. For Co_3O_4@MOF-74, its Faradaic efficiency can be determined from the evolution amount of oxygen gas measured by gas chromatography during electrocatalysis with a fixed current density of 50 mA cm^{-2}. Importantly, the amount of generated oxygen gas matches well with the theoretically calculated value, suggesting a high Faradaic efficiency of >99% during the OER process (**Fig. 4b**). Nyquist plots obtained from the EIS results are also exhibited in **Figure S6**. These plots reveal the enhanced conductivity and smaller resistance after coating the MOF shell layers onto the Co_3O_4 nanowire arrays. The smaller radii of semi-circles at both high and low frequency regions for Co_3O_4@MOF-74 catalysts illustrate the reduced charge transfer resistance and a lower active specie adsorption resistance, significantly promoting the electron transport on the electrode/electrolyte interface and the turnover of absorbed-intermediates into oxygen, as compared with the ones of pristine Co_3O_4. [60–62] Furthermore, the catalytic stability of the samples is also taken into a serious consideration and evaluated using the chronoamperometry method. Under a fixed overpotential of 400 mV, the initial current density is about 67 mA cm^{-2} for Co_3O_4@MOF-74 (without iR correction), while it is only 46 mA cm^{-2} for Co_3O_4. After a testing period of 12 h, the retained current densities become about 65 and 43 mA cm^{-2} for Co_3O_4@MOF-74 and Co_3O_4, respectively, demonstrating that the Co_3O_4@MOF-74 catalyst has the high activity and robust catalytic stability for long-term oxygen evolution (**Fig. 4c**). Moreover, there is not any signif-

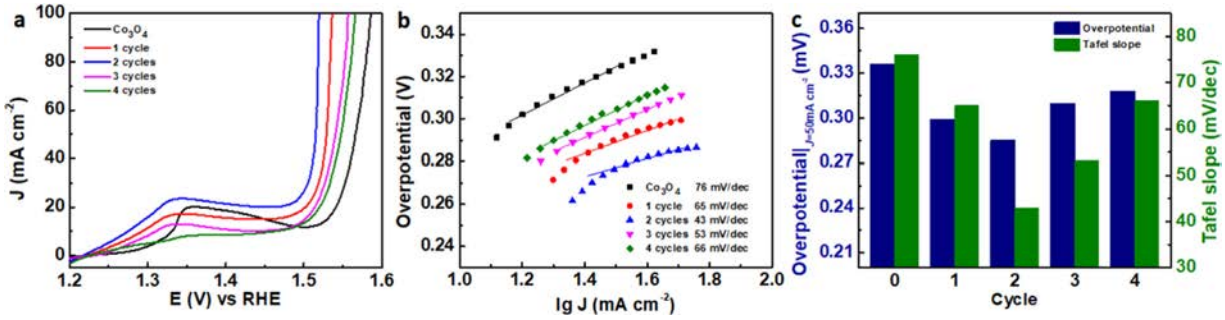

Fig.. 3. Electrochemical activity of Co_3O_4 and Co_3O_4@MOF-74 with various solvothermal cycles. (a) Polarization curves for OER in 1.0 M KOH alkaline solution with scan rate of 10 mV/s. (b) Tafel slopes derived from (a). (c) The dependence of overpotentials (at the current density of 50 mA cm^{-2}) and Tafel slopes with different MOF solvothermal cycles.

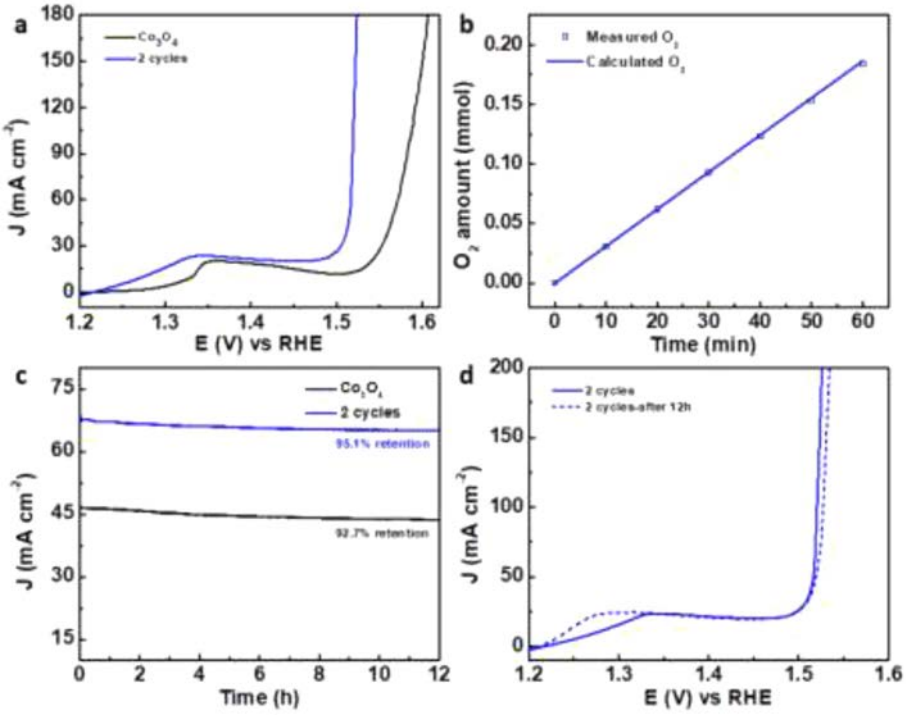

Fig.. 4. (a) Polarization curves for Co_3O_4 and Co_3O_4@MOF-74 with 2 solvothermal cycles in 1.0 M KOH solution. (b) Amount of theoretically calculated and experimentally measured oxygen for Co_3O_4@MOF-74 with 2 solvothermal cycles under the fixed current density of 50 mA cm^{-2} in 1 M KOH solution. (c) Stability tests for Co_3O_4 and Co_3O_4@MOF-74 with 2 solvothermal cycles using the chronoamperometry method (without iR corrections). (d) Polarization curves for Co_3O_4@MOF-74 with 2 solvothermal cycles before and after stability test.

icant deterioration in polarization curves after the stability test for Co_3O_4@MOF-74 (**Fig. 4d**), further revealing the excellent durability of these electrocatalysts.

In previous studies, the activation and transformation of transition metal-based dichalcogenide and phosphide electrocatalysts during the electrocatalytic processes into oxides, oxyhydroxides and hydroxides have been demonstrated (*e.g.* the turnover of metal sulfides into metal oxides) because of the *in situ* oxidation of as-synthesized electrocatalysts during the electrochemical oxygen evolution process, accompanied with oxygen generation. [5, 63] In the case of MOF-based materials during the OER process, similar phenomena should also be taken into account to evaluate any potential changes of MOF structures. For instance, the transformation of Ni-MOF@Fe-MOF into NiO and Fe_2O_3 during the electrocatalytic oxygen generation process in alkaline solution was lately unveiled and thoroughly analyzed, where NiO and Fe_2O_3, instead of the MOF structures, were found to be the actual catalytic centers for OER. [52] A similar finding was as well reported for the case of Ni-based MOFs for oxygen generation and urea oxidation. [64] In this regard, detailed post-reaction characterizations are performed to investigate any changes for the structure of Co_3O_4@MOF-74. HRTEM is employed to learn the morphological and structural properties of the post-reaction sample (**Fig. 5a**, **5b** and **5c**). The morphology of Co_3O_4@MOF-74 after OER stability test is characterized by TEM, as exhibited in **Figure S7** and **Fig. 5a**. TEM images revealed the nanowire-like morphology for Co_3O_4, which was coated with thin shells, as labeled in **Figure S7**. Notably, HRTEM images in **Fig. 5b** and **5c** depicted that the interplanar spacing of 0.237 nm is ascribed to the (101) facet of $Co(OH)_2$, suggesting the $Co(OH)_2$ structured shells on the surfaces of Co_3O_4. FTIR spectra of both Co_3O_4 and Co_3O_4@MOF-74 are as well recorded before and after OER stability test. For pristine Co_3O_4, the peak at 651 cm^{-1} is related to the Co^{2+}—O vibration with the tetrahedral structure in Co_3O_4, [58, 65] where those at 1636 and 3445 cm^{-1} are ascribed to the existence of absorbed molecular water. [65] It is obvious that there is not any significant change in the struc-

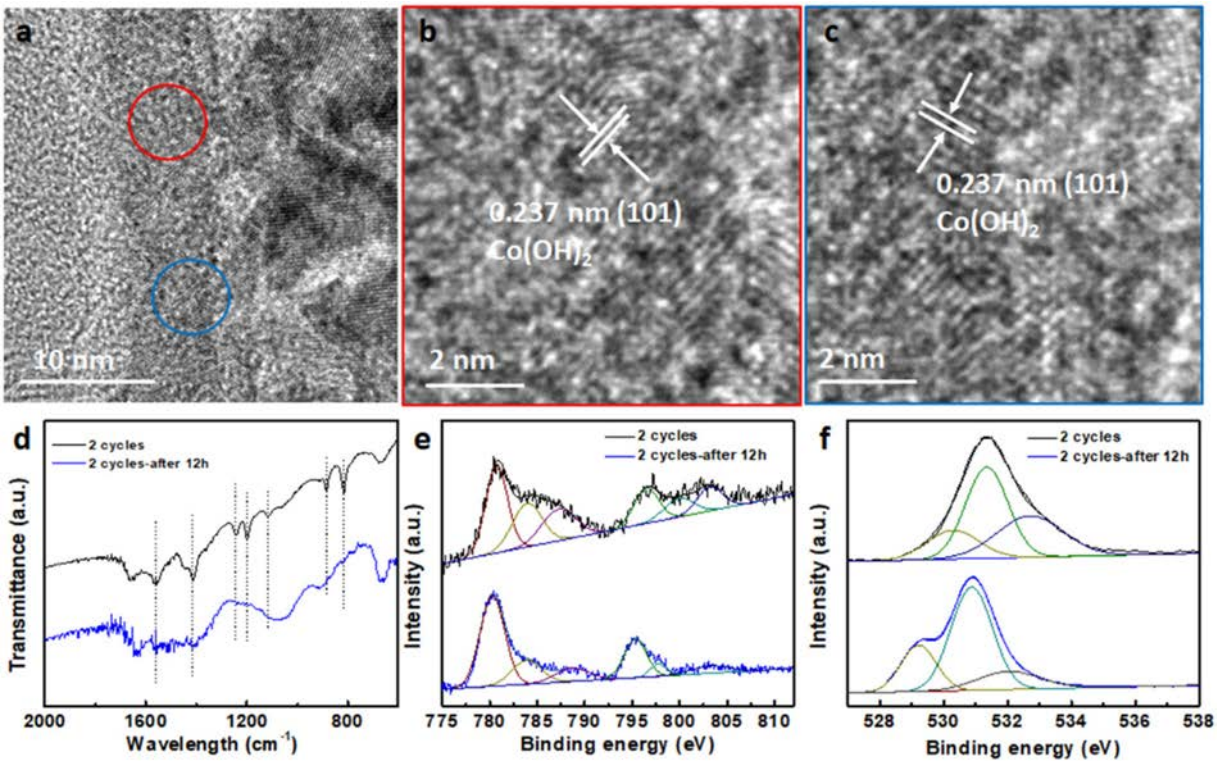

Fig.. 5. (a) HRTEM image of Co_3O_4@MOF-74 with 2 solvothermal cycles after stability test. (b), (c) Corresponding HRTEM images from red and blue color circled regions in (a). (d) FTIR spectra of Co_3O_4@MOF-74 with 2 solvothermal cycles before and after stability test. XPS spectra of (e) Co 2p and (f) O 1 s for Co_3O_4@MOF-74 with 2 solvothermal cycles before and after stability test.

ture of pristine Co_3O_4 after durability test (**Figure S8**). However, Co_3O_4@MOF-74 exhibits noticeable changes with a complete disappearance of above-mentioned characteristic peaks ascribing to the organic ligand of H_4DOBDC and DMF, indicating the loss and breakdown of MOF structures after stability test (**Fig. 5d**). At the same time, XPS spectra of Co and O elements are measured to investigate the changes in chemical states for Co_3O_4@MOF-74 before and after durability test. For Co 2p spectra, peaks at 780.3 and 795.4 eV are attributed to Co^{3+} species, while those located at 784.0 and 797.8 eV are assigned to Co^{2+} species. By integrating the deconvoluted fitting curves, the ratios of Co^{3+}/ Co^{2+} are calculated to be 2.2 and 4.3 for Co_3O_4@MOF-74 before and after stability test, correspondingly. Therefore, more Co^{3+} species are located on the $Co(OH)_2$ surface, serving as catalytic sites for OER. For O 1 s spectra, the significant transformation of chemical structures of Co_3O_4@MOF-74 is witnessed by comparing among the deconvoluted three peaks after stability test. Peaks with the binding energy of 530.3, 531.3 and 532.7 eV are related to the Co—O, *O = C*–O and absorbed water species, respectively [34, 42, 52]. As a result of *in situ* conversion, the electrocatalyst after stability test exhibits three peaks as well, where those at 529.2, 530.9 and 532.1 eV are assigned to the Co—O, Co—OH, and absorbed water species, correspondingly, [52, 66] indicating the preservation of Co—O for the Co_3O_4 core and the transformation into $Co(OH)_2$ species after OER durability test. Based on all these findings, the formation of $Co(OH)_2$ shell layers from MOF-74 is evidently confirmed, in which the *in situ* conversion of Co_3O_4@MOF-74 into Co_3O_4@$Co(OH)_2$ during the electrochemical process for oxygen evolution is consistent with the literature of other similar MOF systems. [52, 64]

In general, Co_3O_4 nanowire arrays on Ni foams are a good type of hard templates for the epitaxial growth of MOF layers on the nanowire surface because of the good conductivity and robust structure. [19] Several unique advantages can be highlighted from this epitaxial synthesis method, followed by the *in situ* conversion of MOF-74 into $Co(OH)_2$ (**Scheme 1**). Firstly, Co_3O_4 is not only the template and substrate to main the vertical structure, but also the metal source to supply Co ions to react with the ligand of H_4DOBDC for the formation of Co-based MOF-74 shell layers without using any other metal sources. This way, the good conductivity of Co_3O_4 as the material core can benefit the transfer of electrons from the electrolyte-electrode interface to the anode. Secondly, the high porosity of MOF-74 shell layers would facilitate the diffusion of alkaline electrolytes to promote its *in situ* electrochemical transformation into a non-compact structure. Once the $Co(OH)_2$ shell is transformed from the MOF-74 layer, there would be an enhanced cohesion between the $Co(OH)_2$ shell and the Co_3O_4 nanowire core, preventing its separation from the core to guarantee the good catalytic stability for OER. Thirdly, the highly-disordered, poor-crystallized and defect-rich $Co(OH)_2$ shell can provide abundant catalytically active sites for the adsorption of active species as well as the subsequent conversion of intermediates. [31, 42] Therefore, designing such metal oxide@MOF core-shell structures can make the most use out of their structural features and their derivatives of metal oxide@metal hydroxide by the *in situ* electrochemical conversion for the excellent and remarkable properties for OER. This presents a valuable insight into the MOF-based materials for electrocatalysis. It is also worth mentioning that, due to the differences and variations of intrinsic chemical properties, some MOF structures are more stable in electrolytes to preserve their initial structural and chemical features. [26, 27, 29] On the other hand, some MOFs may not be stable enough, suffering substantial changes in their structures when operating in alkaline solutions. [49–52] Thus, the post-reaction characterization and analysis of the structure should be carefully performed to evaluate any changes in crystalline and chemical structures during electrochemical processes. All these are essential to understand their

operation mechanisms of MOF-based materials and their nature as effective and stable electrocatalysts.

4. Conclusion

In summary, we have successfully prepared the Co_3O_4@MOF-74 core-shell structure using a template-assisted epitaxial growth method on Co_3O_4 nanowire arrays pre-fabricated on Ni foam substrates. The thickness of MOF shell layers can be simply regulated with a large range by controlling the solvothermal cycles onto the nanowires. The obtained Co_3O_4@MOF-74 samples exhibit remarkably enhanced catalytic properties for OER as compared with pure Co_3O_4 nanowire arrays on Ni foam. Particularly, the Co_3O_4@MOF-74 catalysts, grown with 2 deposition cycles, require a low overpotential of only 285 mV to realize a current density of 50 mA cm^{-2} together with a small Tafel slope of 43 mV/dec. Post-reaction characterizations further demonstrate the transformation of MOF-74 into cobalt hydroxide shell layers, where these *in situ* electrochemically converted cobalt hydroxides are functioned as the actual catalytic centers during the electrocatalytic oxygen generation reaction. Benefitting from these robust core-shell structures, the obtained Co_3O_4@$Co(OH)_2$ electrocatalysts give the excellent durability and activity for OER. This work does not only provide a novel epitaxial growth method of preparing heterogeneous MOF structures, but also unveils the *in situ* transformation mechanism of MOF-based materials during electrochemical reactions, exhibiting a valuable insight into their effective and robust use as electrocatalysts.

5. Credit author statement

J. C. Ho and Y. Ma conceived and supervised the research. J. C. Ho, Y. Ma and W. Gao designed the experiments. J. C. Ho, W. Gao, W. Gou, R. Wei, and X. Bu performed the experiments and data analysis. J. C. Ho, W. Gao, and Y. Ma wrote the paper. All authors discussed the results and commented on the manuscript.

Declaration of Competing Interest

The authors declare no competing financial interest.

Acknowledgements

The authors acknowledged the financial support by the National Natural Science Foundation of China (Grant No. 21401148, 21902128), the Fundamental Research Funds for the Central Universities (3102019QD0406, 3102019JC005), the Science Technology and Innovation Committee of Shenzhen Municipality (Grant JCYJ20170818095520778) and the General Research Fund (CityU 11275916) and the Theme-based Research (T42–103/16-N) of the Research Grants Council of Hong Kong SAR, China.

Supplementary materials

Supplementary material associated with this article can be found, in the online version, at doi:10.1016/j.apmt.2020.100820.

Appendix A. Supplementary data

The following are Supplementary data to this article: additional SEM images, XPS spectra, FTIR spectra, CV curves, and Nyquist plots for Co_3O_4@MOF are exhibited.

References

[1] N.-T. Suen, S.-F. Hung, Q. Quan, N. Zhang, Y.-J. Xu, H.M. Chen, Electrocatalysis for the oxygen evolution: recent development and future perspectives, Chem. Soc. Rev 46 (2017) 337–365.
[2] M. Tahir, L. Pan, F. Idrees, X. Zhang, L. Wang, J.-J. Zou, Z.L. Wang, Electrocatalytic oxygen evolution for energy conversion and storage: a comprehensive review, Nano Energy 37 (2017) 136–157.
[3] G. Liu, Y. Sheng, J.W. Ager, M. Kraft, R. Xu, Research advances towards large-scale solar hydrogen production from water, EnergyChem 1 (2019) 100014.
[4] L. Zhang, B. Liu, N. Zhang, M. Ma, Electrosynthesis of Co3O4 and Co(OH)2 ultrathin nanosheet arrays for efficient electrocatalytic water splitting in alkaline and neutral media, Nano Res 11 (2018) 323–333.
[5] W. Chen, Y. Liu, Y. Li, J. Sun, Y. Qiu, C. Liu, G. Zhou, Y. Cui, In situ electrochemically derived nanoporous oxides from transition metal dichalcogenides for active oxygen evolution catalysts, Nano Lett 16 (2016) 7588–7596.
[6] J.Y. Lee, O.K. Farha, J. Roberts, K.A. Scheidt, S.T. Nguyen, J.T. Hupp, Metal-organic framework materials as catalysts, Chem. Soc. Rev 38 (2009) 1450–1459.
[7] X. Li, X. Yang, H. Xue, H. Pang, Q. Xu, Metal–organic frameworks as a platform for clean energy applications, EnergyChem 2 (2020) 100027.
[8] W. Liu, W.P. Lustig, J. Li, Luminescent inorganic-organic hybrid semiconductor materials for energy-saving lighting applications, EnergyChem 1 (2019) 100008.
[9] B. Zhu, R. Zou, Q. Xu, Metal-organic framework based catalysts for hydrogen evolution, Adv. Energy Mater 8 (2018) 1801193.
[10] J. Liu, D. Zhu, C. Guo, A. Vasileff, S.-Z. Qiao, Design strategies toward advanced MOF-derived electrocatalysts for energy-conversion reactions, Adv. Energy Mater 7 (2017) 1700518.
[11] Y. Chen, S. Ji, Y. Wang, J. Dong, W. Chen, Z. Li, R. Shen, L. Zheng, Z. Zhuang, D. Wang, Y. Li, Isolated single iron atoms anchored on N-doped porous carbon as an efficient electrocatalyst for the oxygen reduction reaction, Angew. Chem. Int. Ed 56 (2017) 6937–6941.
[12] Z.-F. Huang, J. Song, K. Li, M. Tahir, Y.-T. Wang, L. Pan, L. Wang, X. Zhang, J.-J. Zou, Hollow cobalt-based bimetallic sulfide polyhedral for efficient all-pH–value electrochemical and photocatalytic hydrogen evolution, J, Am. Chem. Soc. 138 (2016) 1359–1365.
[13] C. Guan, X. Liu, A.M. Elshahawy, H. Zhang, H. Wu, S.J. Pennycook, J. Wang, Metal-organic framework derived hollow CoS2 nanotube arrays: an efficient bifunctional electrocatalyst for overall water splitting, Nanoscale Horiz 2 (2017) 342–348.
[14] S.H. Ahn, A. Manthiram, Direct growth of ternary Ni-Fe-P porous nanorods onto nickel foam as a highly active, robust bi-functional electrocatalyst for overall water splitting, J. Mater. Chem. A 5 (2017) 2496–2503.
[15] Q. Dong, Q. Wang, Z. Dai, H. Qiu, X. Dong, MOF-derived Zn-doped CoSe2 as an efficient and stable free-standing catalyst for oxygen evolution reaction, ACS Appl. Mater. Interfaces 8 (2016) 26902-2690.
[16] X. Guo, Y. Xu, Y. Cheng, Y. Zhang, H. Pang, Amorphous cobalt phosphate porous nanosheets derived from two-dimensional cobalt phosphonate organic frameworks for high performance of oxygen evolution reaction, Appl. Mater. Today 18 (2020) 100517.
[17] T.Y. Ma, S. Dai, M. Jaroniec, S.Z. Qiao, Metal-organic framework derived hybrid Co3O4-carbon porous nanowire arrays as reversible oxygen evolution electrodes, J. Am. Chem. Soc. 136 (2014) 13925–13931.
[18] X. Wang, H. Xiao, A. Li, Z. Li, S. Liu, Q. Zhang, Y. Gong, L. Zheng, Y. Zhu, C. Chen, D. Wang, Q. Peng, L. Gu, X. Han, J. Li, Y. Li, Constructing NiCo/Fe3O4 heteroparticles within MOF-74 for efficient oxygen evolution reactions, J. Am. Chem. Soc. 140 (2018) 15336–15341.
[19] G. Cai, W. Zhang, L. Jiao, S.-H. Yu, H.-L. Jiang, Template-directed growth of well-aligned MOF arrays and derived self-supporting electrodes for water splitting, Chem 2 (2017) 791–802.
[20] Z. Liang, C. Qu, W. Guo, R. Zou, Q. Xu, Pristine metal-organic frameworks and their composites for energy storage and conversion, Adv. Mater. 30 (2018) 1702891.
[21] C.A. Downes, S.C. Marinescu, Electrocatalytic metal-organic frameworks for energy applications, ChemSusChem 10 (2017) 4374–4392.
[22] S. Zheng, X. Guo, H. Xue, K. Pan, C. Liu, H. Pang, Facile one-pot generation of metal oxide/hydroxide@metal-organic framework composites: highly efficient bifunctional electrocatalysts for overall water splitting, Chem. Commun 55 (2019) 10904–10907.
[23] S. Zheng, Q. Li, H. Xue, H. Pang, Q. Xu, A highly alkaline-stable metal oxide@metal–organic framework composite for high-performance electrochemical energy storage, Nat. Sci. Rev 2 (2020) 305–314.
[24] P.-Q. Liao, J.-Q. Shen, J.-P. Zhang, Metal-organic frameworks for electrocatalysis, Coordin. Chem. Rev 373 (2018) 22–48.
[25] M. Jahan, Z. Liu, K.P. Loh, A graphene oxide and copper-centered metal organic framework composite as a tri-functional catalyst for HER, OER, and ORR, Adv. Funct. Mater 23 (2013) 5363–5372.
[26] S. Zhao, Y. Wang, J. Dong, C.-T. He, H. Yin, P. An, K. Zhao, X. Zhang, C. Gao, L. Zhang, J. Lv, J. Wang, J. Zhang, A.M. Khattak, N.A. Khan, Z. Wei, J. Zhang, S. Liu, H. Zhao, Z. Tang, Ultrathin metal-organic framework nanosheets for electrocatalytic oxygen evolution reaction, Nat. Energy 1 (2016) 16184.
[27] J.-Q. Shen, P.-Q. Liao, D.-D. Zhou, C.-T. He, J.-X. Wu, W.-X. Zhang, J.-P. Zhang, X.-M. Chen, Modular and stepwise synthesis of a hybrid metal-organic framework for efficient electrocatalytic oxygen evolution, J, Am. Chem. Soc. 139 (2017) 1778-178.

[28] J. Duan, S. Chen, C. Zhao, Ultrathin metal-organic framework array for efficient electrocatalytic water splitting, Nat. Commun 8 (2017) 15341.
[29] L. Wang, Y. Wu, R. Cao, L. Ren, M. Chen, X. Feng, J. Zhou, B. Wang, Fe/Ni metal-organic frameworks and their binder-free thin films for efficient oxygen evolution with low overpotential, ACS Appl. Mater. Interfaces 8 (2016) 16736–16743.
[30] X.-.F. Lu, P.-.Q. Liaom J.-W. Wang, J.-.X. Wu, X.-.W. Chen, C.-.T. He, J.-.P. Zhang, G.-.R. Li, X.-.M. Chen, An alkaline-stable, metal hydroxide mimicking metal-organic framework for efficient electrocatalytic oxygen evolution, J. Am. Chem. Soc. 138 (2016) 8336–8339.
[31] L. Tao, C.-.Y. Lin, S. Dou, S. Feng, D. Chen, D. Liu, J. Huo, Z. Xia, S. Wang, Creating coordinatively unsaturated metal sites in metal-organic-frameworks as efficient electrocatalysts for the oxygen evolution reaction: insights into the active centers, Nano Energy 41 (2017) 417–425.
[32] G. Hai, X. Jia, K. Zhang, X. Liu, Z. Wu, G. Wang, High-performance oxygen evolution catalyst using two-dimensional ultrathin metal-organic frameworks nanosheets, Nano Energy 44 (2018) 345–352.
[33] D. Zhu, C. Guo, J. Liu, L. Wang, Y. Du, S.-.Z. Qiao, Two-dimensional metal-organic frameworks with high oxidation states for efficient electrocatalytic urea oxidation, Chem. Commun 53 (2017) 10906–10909.
[34] J. Jiang, L. Huang, X. Liu, L. Ai, Bioinspired cobalt-citrate metal-organic framework as an efficient electrocatalyst for water oxidation, ACS Appl. Mater. Interfaces 9 (2017) 7193–7201.
[35] Y. Xu, B. Li, S. Zheng, P. Wu, J. Zhan, H. Xue, Q. Xu, H. Pang, Ultrathin two-dimensional cobalt-organic framework nanosheets for high-performance electrocatalytic oxygen evolution, J. Mater. Chem. A 6 (2018) 22070–22076.
[36] D.S. Raja, X.-.F. Chuah, S.-.Y. Lu, In situ grown bimetallic MOF-based composite as highly efficient bifunctional electrocatalyst for overall water splitting with ultrastability at high current densities, Adv. Energy Mater 8 (2018) 1801065.
[37] J. Xing, K. Guo, Z. Zou, M. Cai, J. Du, C. Xu, In-situ growth of well-ordered NiFe-MOF-74 on Ni foam by Fe2+ induction as an efficient and stable electrocatalyst for water oxidation, Chem. Commun 54 (2018) 7046–7049.
[38] D. Zhu, J. Liu, L. Wang, Y. Du, Y. Zheng, K. Dvey, S.-.Z. Qiao, A 2D metal-organic framework/Ni(OH)2 heterostructure for an enhanced oxygen evolution reaction, Nanoscale 11 (2019) 3599–3605.
[39] D. Zhu, J. Liu, Y. Zhao, Y. Zheng, S.-.Z. Qiao, Engineering 2D metal-organic framework/MoS2 interface for enhanced alkaline hydrogen evolution, Small 15 (2019) 1805511.
[40] F.-.L. Li, P. Wang, X. Huang, D.J. Young, H.-.F. Wang, P. Braunstein, J.-.P. Lang, Large-scalable, bottom-up synthesis of binary metal-organic framework nanosheets for efficient water oxidation, Angew. Chem 131 (2019) 7125–7130.
[41] W. Cheng, X. Zhao, H. Su, F. Tang, W. Che, H. Zhang, Q. Liu, Lattice-strained metal-organic-framework arrays for bifunctional oxygen electrocatalysis, Nat. Energy 4 (2019) 115.
[42] J. Li, W. Huang, M. Wang, S. Xi, J. Meng, K. Zhao, J. Jin, W. Xu, Z. Wang, X. Liu, Q. Chen, L. Xu, X. Liao, Y. Jiang, K.A. Owusu, B. Jiang, C. Chen, D. Fan, L. Zhou, L. Mai, L. Low-crystalline bimetallic metal-organic framework electrocatalysts with rich active sites for oxygen evolution, ACS Energy Lett 4 (2019) 285–292.
[43] F.-.L. Li, Q. Shao, X. Huang, J.-.P. Lang, Nanoscale trimetallic metal-organic frameworks enable efficient oxygen evolution electrocatalysis, Angew, Chem. Int. Ed 57 (2018) 1888–1892.
[44] C. Cao, D.-.D. Ma, Q. Xu, X.-.T. Wu, Q.-.L. Zhu, Semisacrifcial template growth of self-supporting MOF nanocomposite electrode for efficient electrocatalytic water oxidation, Adv. Funct. Mater 29 (2019) 1807418.
[45] D.S. Raja, H.-.W. Lin, S.-.Y. Lu, Synergistically well-mixed MOFs grown on nickel foam as highly efficient durable bifunctional electrocatalysts for overall water splitting at high current densities, Nano Energy 57 (2019) 1–13.
[46] J. Cao, C. Lei, J. Yang, X. Cheng, Z. Li, B. Yang, X. Zhang, L. Lei, Y. Hou, K. Ostrikov, An ultrathin cobalt-based zeolitic imidazolate framework nanosheet array with a strong synergistic effect towards the efficient oxygen evolution reaction, J, Mater. Chem. A 6 (2018) 18877–18883.
[47] L. Sun, M.G. Campbell, M. Dincă, M. Electrically conductive porous metal-organic frameworks, Angew. Chem. Int. Ed 55 (2016) 3566–3579.
[48] L. Hu, T. Xiong, R. Liu, Y. Hu, Y. Mao, M.-.S. Balogun, Y. Tong, Co3O4@Cu-based conductive metal-organic framework core-shell nanowire electrocatalysts enable efficient low-overall-potential water splitting, Chem. Eur. J. 25 (2019) 6575–6583.
[49] V. Maruthapandian, S. Kumaraguru, S. Mohan, V. Saraswathy, S. Muralidharan, An insight on the electrocatalytic mechanistic study of pristine Ni MOF (BTC) in alkaline medium for enhanced OER and UOR, ChemElectroChem 5 (2018) 2795–2807.
[50] D.O. Miles, D. Jiang, A.D. Burrows, J.E. Halls, F. Marken, Conformal transformation of [Co(bdc)(DMF)] (Co-MOF-71, bdc = 1, 4-benzenedicarboxylate, DMF = N,N-dimethylformamide) into porous electrochemically active cobalt hydroxide, Electrochem. Commun 27 (2013) 9–13.
[51] K. He, Z. Cao, R. Liu, Y. Miao, H. Ma, Y. Ding, In situ decomposition of metal-organic frameworks into ultrathin nanosheets for the oxygen evolution reaction, Nano Res 9 (2016) 1856–1865.
[52] K. Rui, G. Zhao, Y. Chen, Y. Lin, Q. Zhou, J. Chen, J. Zhu, W. Sun, W. Huang, S.X. Dou, Hybrid 2D dual-metal-organic frameworks for enhanced water oxidation catalysis, Adv. Funct. Mater 28 (2018) 1801554.
[53] W.-.W. Zhan, Q. Kuang, J.-.Z. Zhou, X.-.J. Kong, Z.-.X. Xie, L.-.S. Zheng, Semiconductor@metal-organic framework core-shell heterostructures: a case of ZnO@ZIF-8 nanorods with selective photoelectrochemical response, J. Am. Chem. Soc. 135 (2013) 1926–1933.
[54] I. Luz, A. Loiudice, D.T. Sun, W.L. Queen, R. Buonsanti, Understanding the formation mechanism of metal nanocrystal@MOF-74 hybrids, Chem. Mater 28 (2016) 3839–3849.
[55] L. Han, P. Tang, B Álv. Reyes-Carmona, M Rodríguez-García, J.R Torréns, J Morante, J.R Arbiol, Galan-Mascaros, Enhanced activity and acid pH stability of Prussian blue-type oxygen evolution electrocatalysts processed by chemical etching, J. Am. Chem. Soc. 138 (2016) 16037–16045.
[56] K. Tan, S. Zuluaga, Q. Gong, P. Canepa, H. Wang, J. Li, Y.J. Chabal, T. Thonhauser, T. Water reaction mechanism in metal organic frameworks with coordinatively unsaturated metal ions: MOF-74, Chem. Mater 26 (2014) 6886–6895.
[57] R. Wei, M. Fang, G. Dong, C. Lan, L. Shu, H. Zhang, X. Bu, J.C. Ho, High-index faceted porous Co3O4 nanosheets with oxygen vacancies for highly efficient water oxidation, ACS Appl. Mater. Interfaces 10 (2018) 7079–7086.
[58] J. Xu, P. Gao, T.S. Zhao, Non-precious Co3O4 nano-rod electrocatalyst for oxygen reduction reaction in anion-exchange membrane fuel cells, Energy Environ. Sci 5 (2012) 5333–5339.
[59] H. Jiang, Q. Wang, H. Wang, Y. Chen, M. Zhang, Temperature effect on the morphology and catalytic performance of Co-MOF-74 in low-temperature NH3-SCR process, Catal. Commun 80 (2016) 24–27.
[60] J. Jiang, Q. Liu, C. Zeng, L. Ai, Cobalt/molybdenum carbide@N-doped carbon as bifunctional electrocatalyst for hydrogen and oxygen evolution reactions, J. Mater. Chem. A 5 (2017) 16929–16935.
[61] Z. Wang, J. Li, X. Tian, X. Wang, Y. Yu, K.A. Owuwu, L. He, L. Mai, Porous nickel-iron selenide nanosheets as highly efficient electrocatalysts for oxygen evolution reaction, ACS Appl. Mater. Interfaces 8 (2016) 19386–19392.
[62] H. Xu, J.-.X. Feng, Y.-.X. Tong, G.-.R. Li, Cu2O-Cu hybrid foams as high-performance electrocatalysts for oxygen evolution reaction in alkaline media, ACS Catal 7 (2017) 986–991.
[63] J. Ryu, N. Jung, J.H. Jang, H.-.J. Kim, S.J. Yoo, In situ transformation of hydrogen-evolving CoP nanoparticles: toward efficient oxygen evolution catalysts bearing dispersed morphologies with Co-oxo/hydroxo molecular units, ACS Catal 5 (2015) 4066–4074.
[64] V. Maruthapandian, S. Kumaraguru, S. Mohan, V. Saraswathy, S. Muralidharan, An insight on the electrocatalytic mechanistic study of pristine Ni MOF (BTC) in alkaline medium for enhanced OER and UOR, ChemElectroChem 5 (2018) 2795–2807.
[65] X.-.H. Xia, J.-.P. Tu, Y.-.J. Mai, X.-.L. Wang, C.-.D. Gu, X.-.B. Zhao, Self-supported hydrothermal synthesized hollow Co3O4 nanowire arrays with high supercapacitor capacitance, J. Mater. Chem. 11 (2011) 9319–9325.
[66] Z. Chen, C.X. Kronawitter, Y.-.W. Yeh, X. Yang, P. Zhao, N. Yao, B.E. Koel, Activity of pure and transition metal-modified CoOOH for the oxygen evolution reaction in an alkaline medium, J. Mater. Chem. A 5 (2017) 842–850.